Hindawi
International Journal of Aerospace Engineering
Volume 2023, Article ID 2407730, 18 pages
https://doi.org/10.1155/2023/2407730

Research Article

Biaxial Tensile Mechanical Properties of HTPB Solid Propellant

Li Jin, Qinzhi Fang, Xingwei Yan, and Qinwei Hu

State Key Laboratory for Strength and Vibration of Mechanical Structures, Department of Engineering Mechanics, Xi'an Jiaotong University, Xi'an 710049, China

Correspondence should be addressed to Li Jin; jinli5074@stu.xjtu.edu.cn

Received 11 March 2023; Revised 22 September 2023; Accepted 25 September 2023; Published 6 October 2023

Academic Editor: Qingfei Fu

The purpose of this work is to study the effects of different loading rate ratios and loading speeds on the biaxial tension of hydroxyl-terminated polybutadiene (HTPB) solid propellant. A proper kind of biaxial tensile specimen with which the stresses in its central part can be obtained with the loads acted on each loading direction is designed and used in the study, and the strains in its central parts are obtained with the digital image correlation (DIC) method. The stress and strain relationship at each direction can be obtained by experiments. The uniaxial stress vs. strain curves and the biaxial stress vs. strain curves were obtained, and it was found that the loading speed remarkably influenced the biaxial tensile behaviors of HTPB propellant. The Mises equivalent stress and strain could be used to describe the biaxial tension stress and strain state, and the exponential constitutive model obtained in the study could be used to predict the stress vs. strain curve under different test conditions.

1. Introduction

In the course of manufacturing, storage, transportation, ignition, and flight, solid rocket motor (SRM) grain was exposed to stresses such as heat, impact, vibration, acceleration, and ignition pressure [1–3]. If the grain's stress and strain levels exceeded acceptable levels, damages like grain fracture, deformation, and other things could happen. This would seriously impair the SRM's working performance and could even result in the engine's total destruction [4, 5]. It is necessary to determine the materials' permissible limits for stress and strain in order to evaluate the SRM's structural integrity. The structural integrity study of grain is based on research on the mechanical characteristics and constitutive model of solid propellant [6–9]. External temperature, loading strain rate, and loading mode all had a clear impact on the mechanical characteristics of solid propellants [10–12]. To inform the structural design of grain and guarantee the appropriate operation of SRM, research on the mechanical characteristics and constitutive model of solid propellants under various loading circumstances was of major value [13]. The mechanical characteristics of propellant and its deterioration under various loading circumstances have received a lot of attention [14, 15]. Temperature, stress and strain condition, etc., all have a significant impact on the mechanical characteristics and fracture mechanisms of solid propellants [16].

In order to understand the behavior of composite propellants during engine ignition, the mechanical and ultimate performance of propellants filled with water-terminated polybutadiene were studied under imposed hydrostatic pressure [17]. The mechanical response of the propellant was obtained by uniaxial tensile and simple shear tests at several temperatures, strain rates, and superimposed pressures from atmospheric pressure to 15 MPa. The difficulty of directly measuring stress in solid propellants was noted and discussed. In order to evaluate the stress in solid propellants, the piezoresistive phenomenon was explored and demonstrated [18]. The uniaxial compressive mechanical response of two high-energy polymer propellants, M30 and JA2, was studied using statistical factor design techniques. It was found that the aspect ratio and end lubrication variables can affect the overall mechanical behavior of these materials [19]. The stress vs. strain curve and tensile fracture surface of

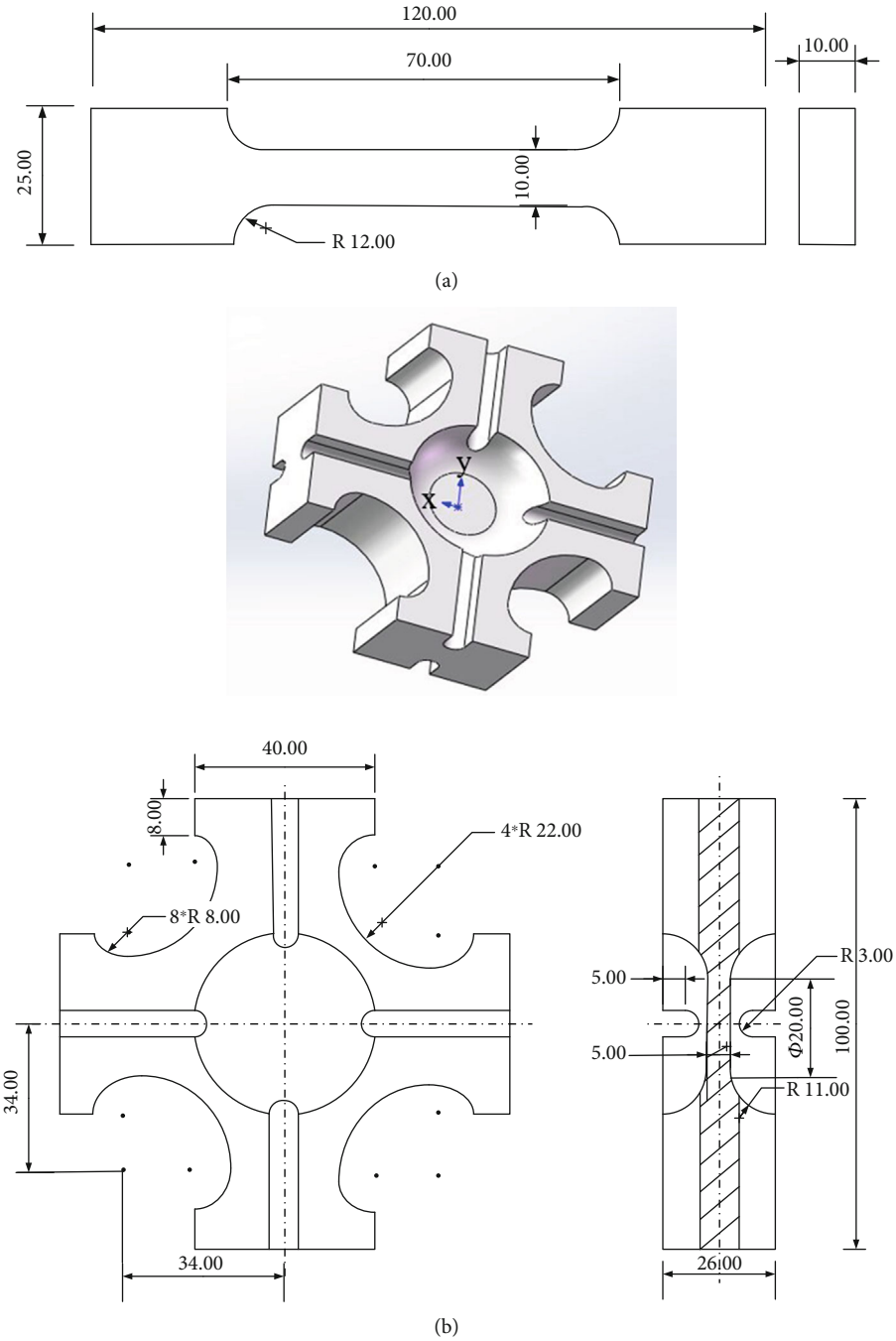

Figure 1: Schematic diagram of the HTPB propellant test sample: (a) uniaxial tensile test sample (mm) and (b) biaxial tensile test sample (mm).

HTPB propellant were studied using uniaxial and biaxial tensile tests over a wide range of temperature and strain rates, respectively. The results indicate that the strength of the material increases with the decrease of environmental temperature and the increase of loading strain rate [20, 21]. Previous studies have shown that uniaxial testing could not determine the accurate mechanical properties of high particle-filled elastomers subjected to complex loads. Therefore, conducting uniaxial tests of solid propellants alone could not meet the research requirements for the mechanical properties of solid propellants.

In fact, the loading of solid propellants during storage and transport is very complex. In recent decades, attempts have been made to investigate the mechanical properties of materials under biaxial loading using a variety of specimens and loading devices. The study of viscoelastic properties as well as the effect of softening and the occurrence of induced anisotropy in filled elastomers was completed by biaxial loading tests using a four-vector test rig, the Zwick/Roell test machine [22]. The effect of vertical tensile load and bidirectional tensile load ratio on the mechanical properties of single-ply nylon rope and rubber composites under

bidirectional tensile conditions was investigated [23]. A new test fixture that can be used for biaxial compression tests on a uniaxial testing machine was designed, and the biaxial compression behavior of polymer foam was investigated [24]. To design and improve the protective properties of Kevlar 49 fabrics, the stress-strain response, the apparent Poisson's ratio, and the in-plane shear response of Kevlar 49 fabrics in the warp and weft directions were investigated by biaxial tensile tests. The experimental results showed that it has the same Young's modulus in the warp and filling directions, but different curl strains, tensile strengths, and ultimate strains [25]. A newly designed aluminum apparatus and uniaxial Instron tester were used [26]. Then, quasibiaxial tensile stress responses were obtained for HTPB propellants at room temperature and at different high strain rates. Based on the above studies, it can be seen that the biaxial tensile test type has been developed through the biaxial tensile test of film convex expansion, biaxial tensile test of internally pressed thin-walled cylinders or spherical shells, and biaxial tensile test of plane cross-shaped specimens [27–30]. Comparison of the results of their research can be seen, cross-shaped specimen biaxial tensile results are closer to the mechanical properties of materials subjected to complex loads, and cross-shaped biaxial tensile test to promote the development of biaxial tensile testing machine, especially the plane cross-shaped specimen for biaxial tensile test, has the advantages of frictionless, measurement of noncontact, and so on, and at the same time, changing the two-axis loading displacement ratio can be obtained by the different strain paths of linear or nonlinear. At the same time, by changing the loading displacement ratio of the two axes, the linear or nonlinear equivalent force strain curves of different strain paths can be obtained, which is very popular. However, there are few studies on the biaxial tensile experiments on cross specimens of solid propellant HTTP. So far, the main conclusions of the biaxial mechanical property studies on solid propellant HTPB are based on quasibiaxial mechanical experiments [10, 20]. Since the quasibiaxial experiments cannot control the loading rate ratio in both directions very accurately, it is doubtful whether the results of quasibiaxial experiments can accurately reflect the biaxial mechanical properties. In reality, the biaxial loading to which the material is subjected is complex and varied, in which the nonequivalent biaxial loading is dominant, and the nonequivalent loading situation cannot be skipped in the study of the biaxial mechanical properties. Due to experimental difficulties, it is difficult to effectively obtain the biaxial tensile behavior of solid propellant materials. Quasibiaxial stretching can only obtain biaxial tensile properties of the material for which the equivalent load ratios are approximated. Biaxial tests on solid propellant butyl hydroxyl propellants with different load ratios have not been successfully carried out and do not provide relevant mechanical properties. Therefore, in order to gain a comprehensive understanding of solid propellants, this work will investigate the biaxial tension of solid propellants at different load ratios.

At present, quasistatic biaxial tensile mechanical property tests of solid propellants can be divided into two categories according to the type of experimental setup. One type is the uniaxial tensile testing machine with strip specimens [31]. The other type is the biaxial tensile testing machine test method with crossed specimens [32]. Crossed specimens are more suitable for biaxial tensile tests due to the biaxial tensile limitations of strip specimens [33–36]. Due to the low modulus and low strength physical properties of solid propellants, as well as the high level of risk and the complex carving process of solid propellant cross-shaped specimens, measures such as center thinning or slotting in the arm alone are not well suited to improve the reliability of biaxial tensile mechanical property testing of cross-shaped specimens [37].

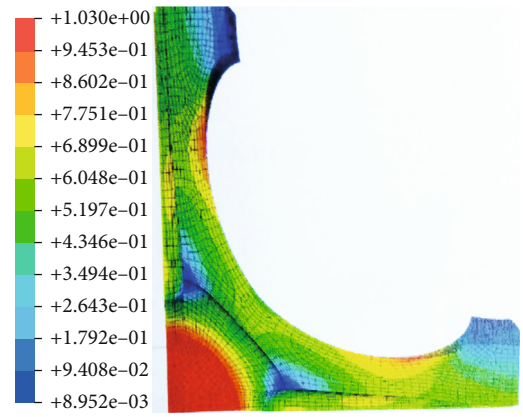

Figure 2: Mises stress of test piece under 20% strain.

In this paper, the biaxial stretching experiment of hydroxyl-terminated polybutadiene (HTPB) propellant at two different loading speeds, four kinds of loading rate ratios, and at room temperature is going to be performed. A newly designed cruciform sample with a reduced center section and slots is used. The relationship between load and stress in the central portion of the specimen in each corresponding direction is obtained by means of the linear viscoelastic intrinsic structure that comes with ABAQUS. The tensile behaviors of HTPB propellant under different loading speed and different loading rate ratios are discussed, and a constitutive equation is established.

2. Experimental

2.1. Material. The test material was HTPB solid rocket propellant, and the matrix was a viscoelastic material and contains metal particles. The solid propellant consisted of AP (ammonium perchlorate, 69.50 wt. %) as an oxidizer, Al (aluminum powder, 18.50 wt. %) powders as a metal fuel, DOS (di-2-ethylhexyl sebacate, 3.40 wt. %) as a plasticizer, MAPO (tri-(2-methylaziridinyl) phosphine oxide, 0.05-0.10 wt. %) as a bonding agent, TDI (2,4-toluene diisocyanate, 1.0-2.0 wt. %) as a curing agent, HTPB (hydroxyl-terminated polybutadiene, 0.6-0.7 wt. %) as a binder, and additives (liquid, 0.50-1.0 wt. %). Moreover, the sizes of larger ammonium perchlorate (AP) particles were within the range of 100–400 μm in diameter. The sizes of smaller AP particles were less than 35 μm in

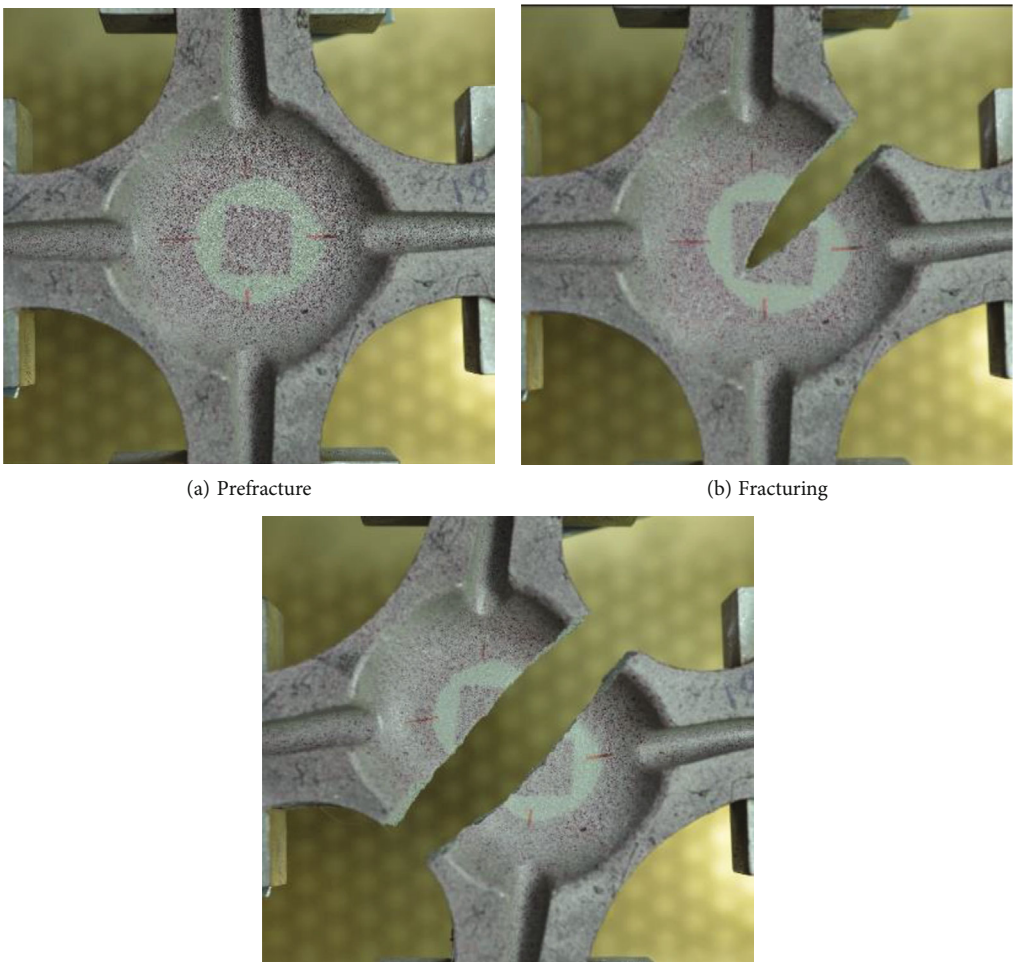

(a) Prefracture (b) Fracturing

(c) Complete fracture

Figure 3: Failure process of propellant specimen.

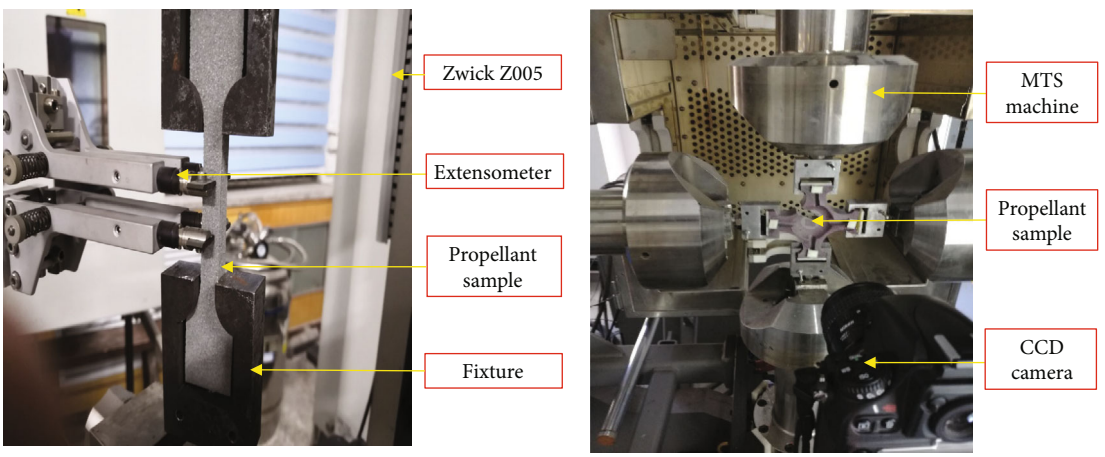

(a) (b)

Figure 4: (a) Uniaxial tensile instruments and specimen. (b) Biaxial apparatus used for biaxial experiments with the cruciform shape specimen.

Table 1: The test conditions.

Type of test	Test instrument	Test temperature (°C)	Test number	Displacement loading speed (mm/min)		Number of tests
				X direction	*Y* direction	
Uniaxial	Zwick Z005	23	U1-1, U1-2, U1-3	/	1	3
			U2-1, U2-2, U2-3	/	2	3
			U20-1, U20-2, U20-3	/	20	3
Biaxial	MTS		B5, B18	2	2	2
			B19, B25	1	2	2
			B20, B24	0.667	2	2
			B22, B31	0.5	2	2
			B10, B17	100	100	2
			B11, B30	50	100	2
			B9, B14	33.33	100	2
			B13, B29	25	100	2

diameter. The mean size of aluminum particles was 22 μm. These components eventually form an over reticulated HTPB matrix.

2.2. Sample Preparation. Biaxial tensile test is the extension and expansion of uniaxial tensile test, so in the study of biaxial tensile properties, it is indispensable to compare the results of biaxial tensile test with the results of uniaxial tensile test. According to the Chinese aerospace industry standard, GJB 770B-2005, the uniaxial tensile sample was designed as a type B dumbbell shape, as shown in Figure 1(a). But there were no standard available for the dimensions of biaxial tensile sample. Based on the previous research, a new sample was designed which was slotted on the arm and widened the radius of the arc segment. A schematic diagram of the cruciform sample is shown in Figure 1(b).

The following are the benefits and enhancements of the biaxial tensile specimens developed in this paper as opposed to earlier specimens, as shown by the biaxial specimen diagram in Figure 1(b):

(1) Compared to previous biaxial tensile specimens [38, 39], the center of the specimen in this paper has been reduced to a very thin thickness of 5 mm, which can achieve significant deformation at the center

(2) In the past, the shear stress in the middle area was removed from the wall using just one groove to simplify the operation, but the results were not satisfactory. Due to this, two grooves with a 3 mm radius were carved into the specimen's wall. As a result, the shear stress in the central region will be significantly reduced or even eliminated, causing the central deformation zone's stress primary axis to coincide with the tensile direction. The major tension in the central region may be measured and calculated more easily using this groove

(3) As opposed to earlier biaxial examples, each corner of the specimen only had one chamfered corner. Large shear stresses at the individual chamfered corners can cause unequal positive stresses in the central zone and deviate from the direction of tension, which leads to mistakes in the calculation of stresses in the central zone. Shear stresses can also extend towards the central zone as a result. Each corner of the biaxial specimens in this paper has two 8 mm radius chamfered corners. This will significantly lower the shear stress at the corners and hence lower the stress in the central zone calculation error

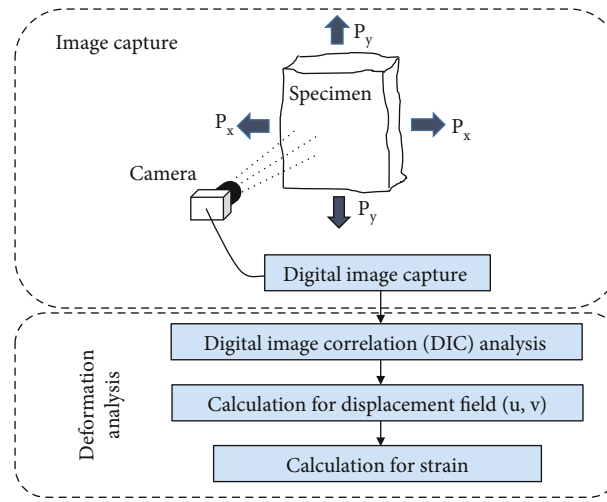

Figure 5: Block diagram of the deformation measurement system.

In order to verify the validity of the newly designed biaxial tensile specimen, this paper uses numerical simulation calculations and test pictures. The deformation of 1/8 finite element model of cross biaxial tensile cruciform specimen with different loading rate ratios is calculated and analyzed by using ABAQUS software. Figure 2 shows the Mises stress diagram of the specimen at 20% strain under isometric biaxial tensile loading. In the calculations, the propellant is modelled by the "Prony series" viscoelastic structure model with

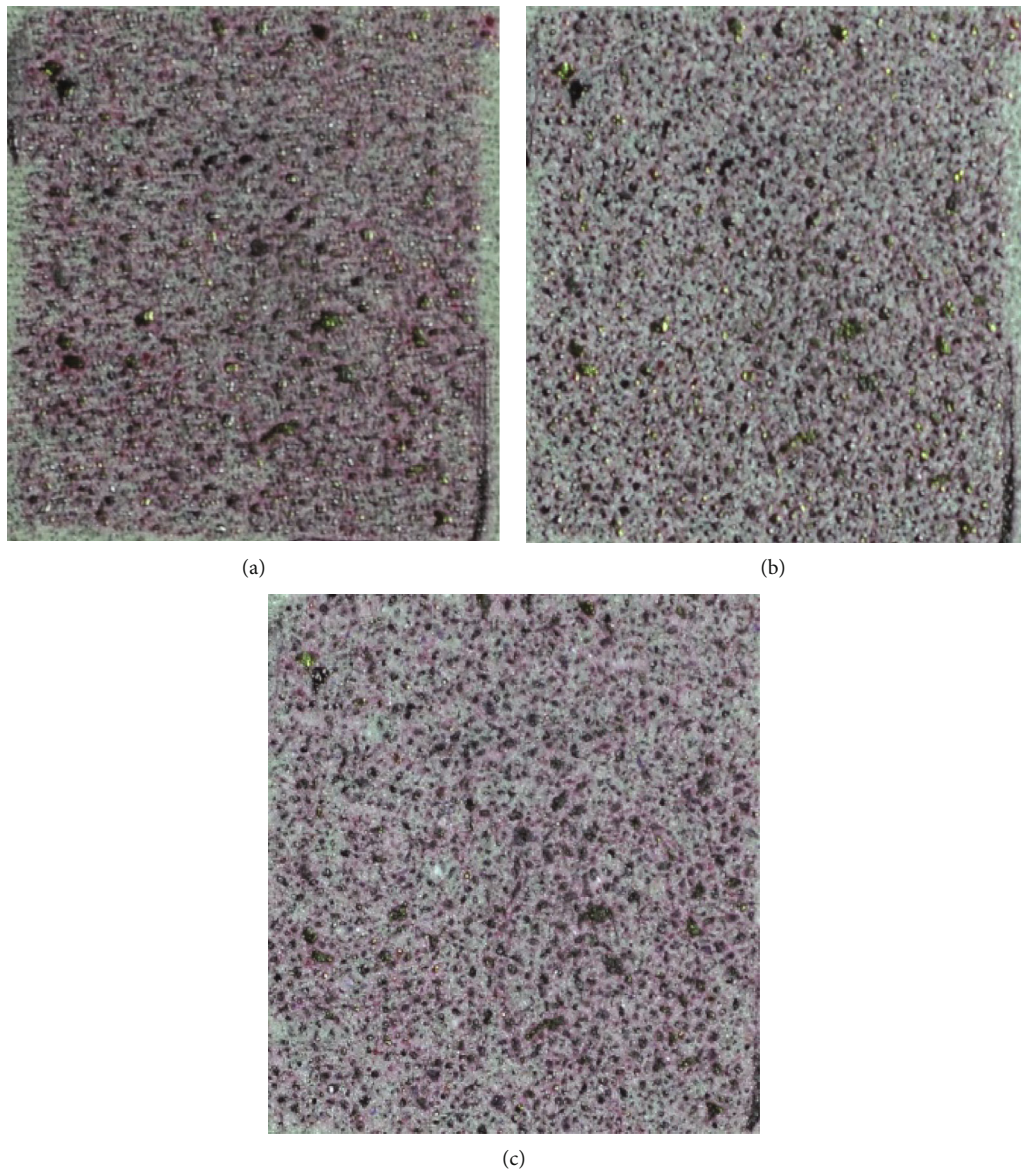

(a) (b) (c)

Figure 6: Front view images of HTPB tensile specimen at different times: (a) image corresponding to $t = 0$ s, (b) image corresponding to $t = 540$ s, and (c) image corresponding to $t = 600$ s.

Poisson's ratio of 0.495 and a mesh of C3D8RH mesh elements. From Figure 2, it can be seen that the maximum stress occurs in the central region, and the stress value in this region is generally larger than that in the noncentral region, which is sufficient to ensure that the specimen is damaged from the central region. In addition, the stress concentration in the central region is not obvious.

By photographing the tensile damage process of specimen B18 under 1 : 1 axial loading, as shown in Figure 3, the cracks expanded towards the corners of the specimen limbs until they ran through the whole specimen. The tensile load on the specimen limbs forms a resultant force in the central region of the specimen, i.e., the tensile loads at the two adjacent ends are combined to form a larger load pointing in the direction of the chamfered corners of the limbs, which causes the specimen to fracture along the chamfered direction of the limbs. At the same time, the central region of the specimen is the thinnest part of the whole specimen, while the joints of the specimen limbs are relatively thick, so the crack initiation point of the specimen occurs in the relative central region of the specimen. The fracture behavior is in accordance with the expected results of the isometric biaxial tensile test. Combined with Figures 2 and 3, it can be seen that the newly designed biaxial tensile specimen is effective and can meet the test requirements.

2.3. Experiment. The newly designed biaxial tensile specimens processed in this paper were produced using a casting production method with the highest degree of fault tolerance. Firstly, the HTPB propellant formulation shown in section 2.1 was mixed proportionally at 58°C. The release

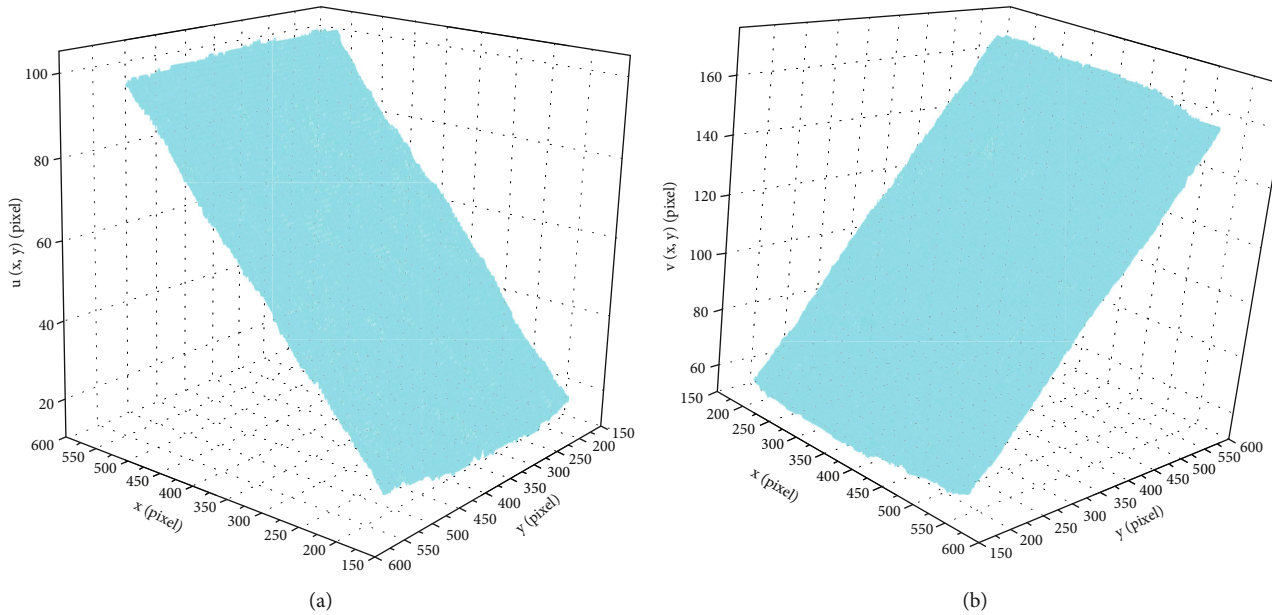

(a) (b)

FIGURE 7: Displacement fields at the time $t = 540$ s for the specimen B5: (a) displacement field $u(x, y)$ in X direction and (b) displacement field $v(x, y)$ in Y direction.

agent was applied to the surface of the custom mould coated with the release agent, and then, the mixed propellant slurry was poured into the mould. Finally, the mould is placed at a constant temperature of 20°C, and the propellant sample is removed after the slurry has completely solidified. After processing, the specimen is placed in a drying oven for drying. Due to the most fault-tolerant casting production method, initial damage to the specimen during processing is almost negligible and does not affect the accuracy of subsequent test results.

The uniaxial tensile test was carried out on a universal test machine Zwick Z005 at a room temperature of approximately 23°C, as shown in Figure 4(a). An extensometer and load cell were used to record the deformation and the load acted on the uniaxial tensile specimen simultaneously. The biaxial tensile test was carried out on the MTS biaxial tensile testing machine, as shown in Figure 4(b), the load cells in each direction record the load acted on each arm of the cruciform specimen. The deformation of the center part of the cruciform specimen was obtained with camera, and the strains vs. time in each direction were calculated with the digital image correlation (DIC) method.

The experiments were performed with displacement control. The uniaxial tension experiment was carried out at three displacement loading speeds of 1 mm/min, 2 mm/min, and 20 mm/min, respectively. The biaxial experiment was carried out with four different loading rate ratios and two different loading speeds in the Y direction. The specific implementation method was to apply 2 mm/min and 100 mm/min displacement loading speed in the Y direction. For the displacement loading speed of 100 mm/min in the Y direction, by changing the displacement loading speed in the X direction, such as applying 100 mm/min, 50 mm/min, 33.33 mm/min, and 25 mm/min in the X direction, then the loading rate ratios of $X:Y$ of 1:1, 1:2, 1:3, and 1:4 could be gotten. For the displacement loading speed of 2 mm/min in the Y direction, the displacement loading speeds in the X direction were applied with 2 mm/min, 1 mm/min, 0.666 mm/min, and 0.5 mm/min, respectively, to get the loading rate ratios of $X:Y$ of 1:1, 1:2, 1:3, and 1:4 loading scheme. The test conditions have been listed in Table 1, which includes the test number specimen and the loading method, as follows.

A Nikon D800 camera was used to take pictures. For the test with a loading rate of 100 mm/min in the Y direction, the photo interval was one second for one picture. About the test with a loading rate of 2 mm/min in the Y direction, the photo interval was five seconds a picture. To give a better characterization of the specimen surfaces, random speckle pattern with two different colors (black and red) was sprayed onto the specimen surface in the center part.

2.4. DIC Method. The digital image correlation (DIC) method was adopted to measure the displacement field of the center part of the cruciform specimen during the biaxial tensile test. The principle of the DIC method was given in reference [40]. The principal features and procedures of the displacement measurement system were developed in this paper as shown in Figure 5.

2.5. Linear Viscoelasticity. In order to obtain the relationship between the load applied to the specimen arms and the stress in the central portion of the specimen, this paper is carried out by using the linear viscoelastic material [41] model that comes with the finite element software ABAQUS. By simulating the loading conditions with different displacement loading rates, the relationship between loads and stresses in all directions of HTPB composite solid propellant can be obtained.

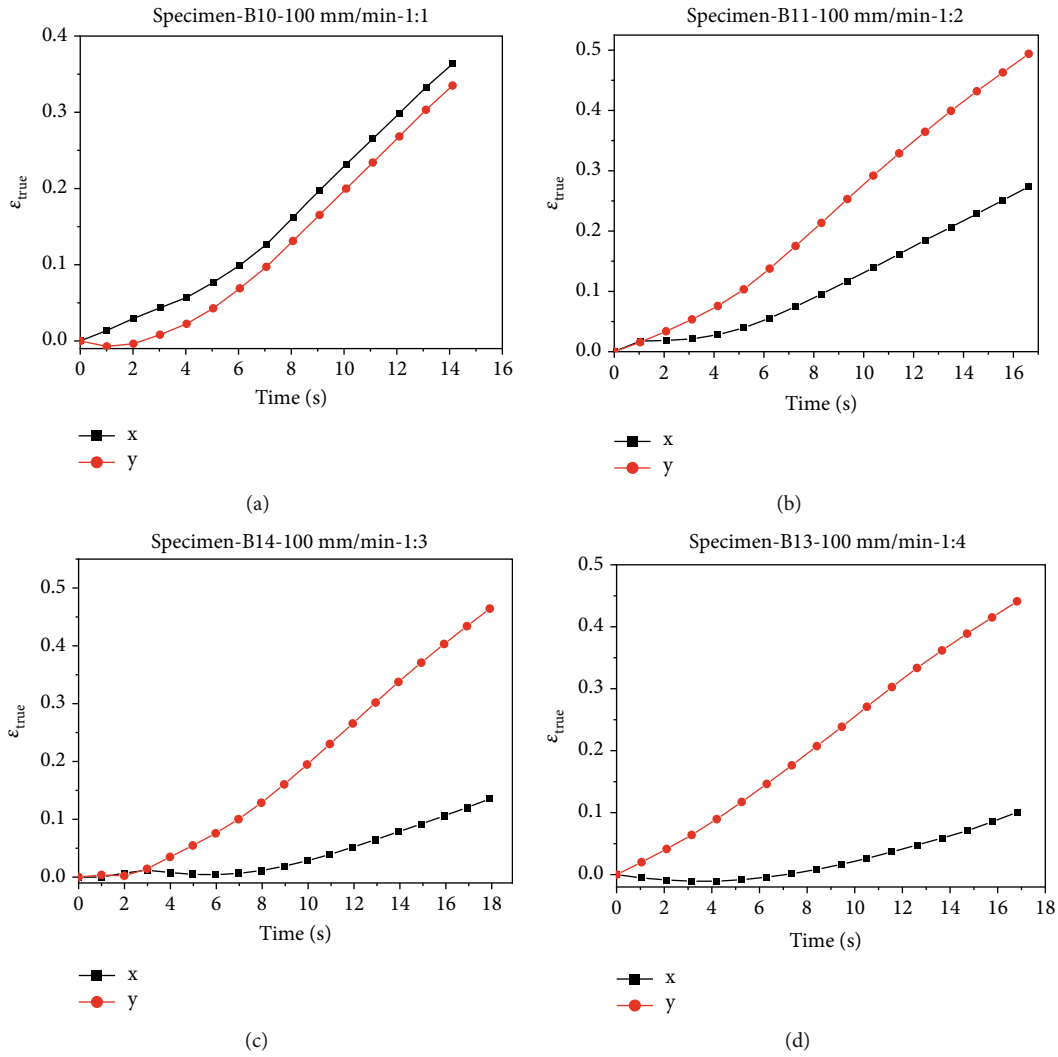

FIGURE 8: Strain (true) vs. time curves of the biaxial tensile tests for HTPB propellant at 100 mm/min displacement loading speed: (a) strain (true) vs. time curve with loading rate ratio of 1 : 1, (b) strain (true) vs. time curve with loading rate ratio of 1 : 2, (c) strain (true) vs. time curve with loading rate ratio of 1 : 3, and (d) strain (true) vs. time curve with loading rate ratio of 1 : 4.

The constitutive model chosen for this paper is the time-based integral constitutive model as follows:

$$\sigma(t) = E(t)\varepsilon_0 + \int_{0^+}^{t} E(t-\tau)\frac{d\varepsilon(\tau)}{d\tau}d\tau = \int_{0}^{t} E(t-\tau)\frac{d\varepsilon(\tau)}{d\tau}d\tau, \tag{1}$$

where σ is the stress, ε is the strain, t is the time, and $E(t)$ is the relaxation modulus equation. The relaxation modulus in this paper is expressed in terms of a Prony series of the third order, as follows:

$$E(t) = 0.97508 + 0.23156e^{-t/2.04804} + 0.15216e^{-t/39.1531} + 0.17785e^{-t/640.4452}. \tag{2}$$

It is sufficient to input each relaxation modulus and its corresponding relaxation time constant in Eq. (2) into the model built in ABAQUS to give the model linear viscoelastic material properties.

3. Results and Discussion

3.1. Biaxial Tensile Displacement Measurement. The images of the center part of the cruciform specimen recorded with camera during experiment were processed with the DIC program, and the displacement field vs. time could be obtained.

Figure 6 shows three of the images of solid propellant HTPB biaxial tensile No. 5 specimen (abbreviated as B5) which were the images of the center part of the cruciform specimen. It was shown that the area of the center part of the specimen increases with the time of the biaxial tension test.

With the image shown in Figure 6(a) as the initial image at $t = 0$ s, the displacement fields $u(x, y)$ in X direction and $v(x, y)$ in Y direction for the picture shown in Figure 6(a),

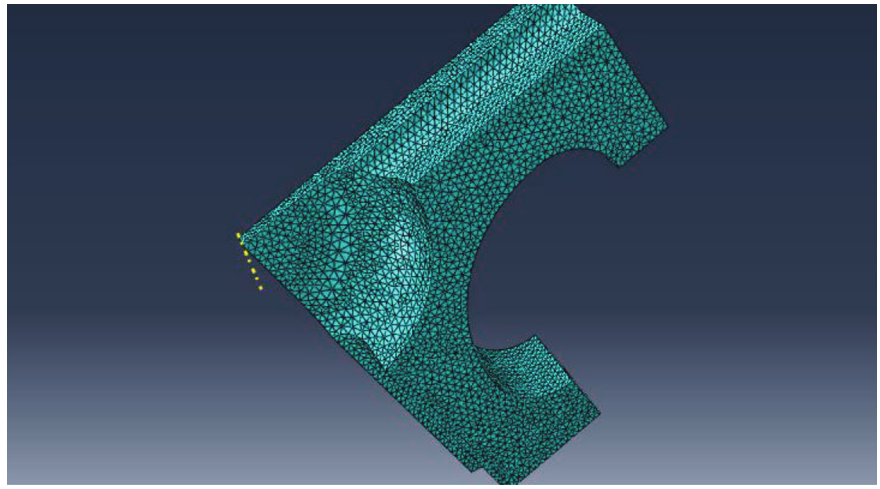

Figure 9: 1/8 finite element model of cross biaxial tensile specimen.

respectively, were obtained with DIC method, and the results are given in Figures 7(a) and 7(b). The unit of the displacements u, v, x, and y was pixel. It was shown from Figure 7 that the displacement fields in the x and y direction in the central part of the specimen were approximately plane; therefore, the strain field in the central region of the specimen was approximately uniform. So, the design of the specimen shown in Figure 1(b) was suitable for the biaxial tensile experiment. The average strain in this region could be used to represent the strain in the central part of the specimen.

3.2. Biaxial Tensile Strain Calculation. The main purpose of this paper was to obtain the stress and strain relationship of HTPB solid propellant. It could be seen from Figure 7(a) that the displacement field in X direction $u(x, y)$ was nearly related only with the coordinate of x and nearly had no effect with the coordinate of y. By linear fitting $u(x, y)$ to the coordinates x and y, respectively, the results were shown as follows:

$$u(x, y) = -25.21939 + 0.22794x, \tag{3}$$

$$u(x, y) = 57.97016 + 0.0000268681y. \tag{4}$$

It was proved from Eqs. (3) and (4) that the displacement field in X direction $u(x, y)$ had a strong linear relationship with the coordinate x but had almost no effect with the y position. The slope in Eq. (3) was the engineering strain in the X direction, and its value was $(\varepsilon_x)_{t=540} = 0.22794$. Similarly, the engineering strain in the Y direction could also be obtained by linear fitting the displacement field in Y direction $v(x, y)$ with the coordinate y, the engineering strain in the Y direction $(\varepsilon_y)_{t=540}$ could be obtained, and its value was $(\varepsilon_y)_{t=540} = 0.30242$. The tensile true strains in the two lateral directions could be calculated as

$$(\varepsilon_{\text{true}})_x = \ln(1 + \varepsilon_x), \tag{5}$$

$$(\varepsilon_{\text{true}})_y = \ln(1 + \varepsilon_y). \tag{6}$$

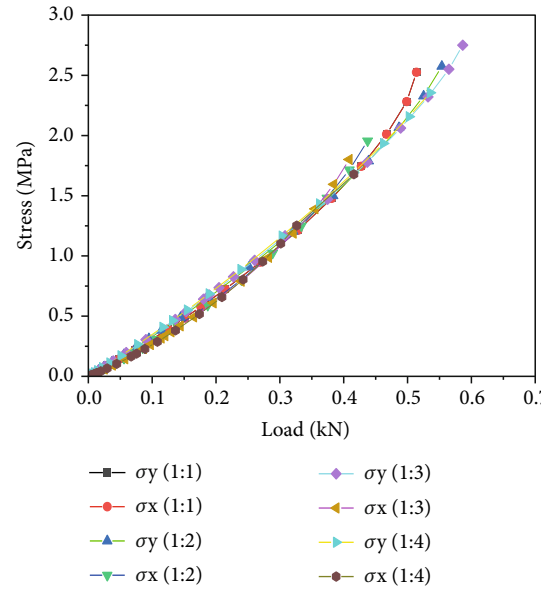

Figure 10: The stress vs. load curve under four loading rate ratios.

By calculating all the images taken during the biaxial tension process, the displacement fields and the corresponding strains in the center part of the all specimens at different times could be obtained. So that, the strain (true)-time curves for all the specimens could be gotten.

Parts of the strain (true) vs. time curves with four loading rate ratios for the specimens tested with the displacement loading speed of 100 mm/min are shown in Figure 8. From the strain (true) vs. time curves shown in Figure 8, it could be seen that the ratio of true strain in the two directions at different times had a little different with the displacement loading rate. For example, in Figure 8(a), the ideal strain (true) vs. time curves in x and y directions should be the same; although the tendency of the curves was the same, the value of the strains in x and y directions at the same time had a little difference. This difference was caused by that the loading in two directions could not be exactly synchronous.

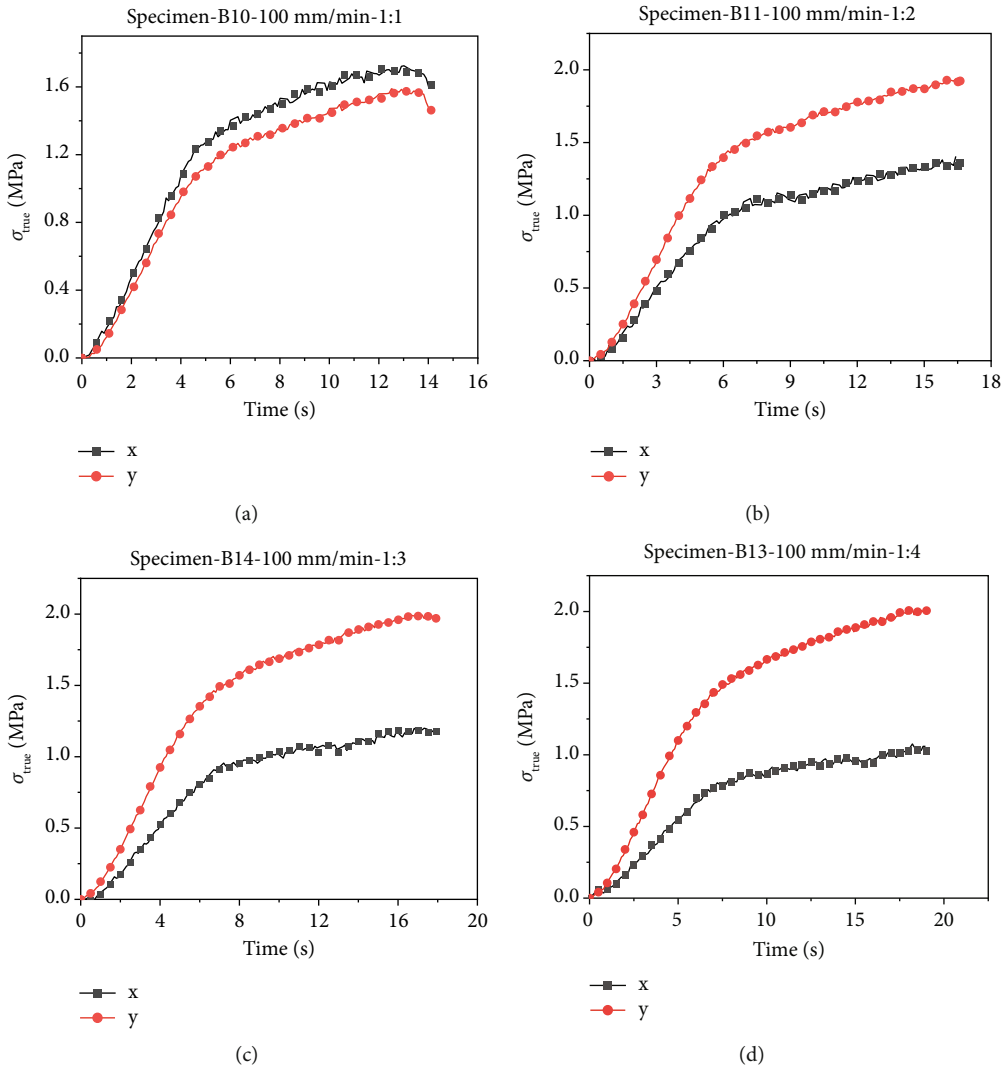

Figure 11: Stress (true) vs. time curves of the biaxial tensile tests for HTPB propellant at 100 mm/min displacement loading speed: (a) stress (true) vs. time curve with loading rate ratio of 1 : 1, (b) stress (true) vs. time curve with loading rate ratio of 1 : 2, (c) stress (true) vs. time curve with loading rate ratio of 1 : 3, and (d) stress (true) vs. time curve with loading rate ratio of 1 : 4.

3.3. Biaxial Tensile Stress Calculation. During the experiment, the values of the loads P_x and P_y in both directions could be recorded directly on the MTS experimental machine. In order to obtain the stresses in the center part of the specimens tested, a cross-sample model shown in Figure 1(b) corresponding to the 1 : 1 size of the experimental sample is established. Due to its symmetry, in order to simplify the calculation, a 1/8 model was established, as shown in Figure 9.

The simulations of the biaxial loading with different displacement loading rate ratios were done. The relationship of the load acted on the arms of the specimen and the average stresses in the corresponding directions for four different loading rate ratios are obtained and shown in Figure 10.

From the stress vs. load calculation results in Figure 10, it could be found that the stresses in the central part were only related to the load acted on the arms of the specimen and nearly not related with the loading rate ratios. It was a very useful result that we could get the stresses in the center part with the load acted on the arms of the specimen, regardless of the deviation of the loading rate ratio in a real experiment (such as that in Figure 8). The relationship between the average stress in the central region and the load acted on the arms of the specimen in the corresponding directions could be obtained by fitting the data shown in Figure 10 and was given as Eq. (6).

$$\sigma = 3.74445P^2 + 2.58825P. \tag{7}$$

The unit of stress σ is MPa, and the unit of load P is kN.

With the load acted on each arm of the specimen, the stresses in the center part of the specimen in X and Y direction, respectively, could be obtained with Eq. (7), so that the stress vs. time curves could be drawn. Figure 11 shows parts

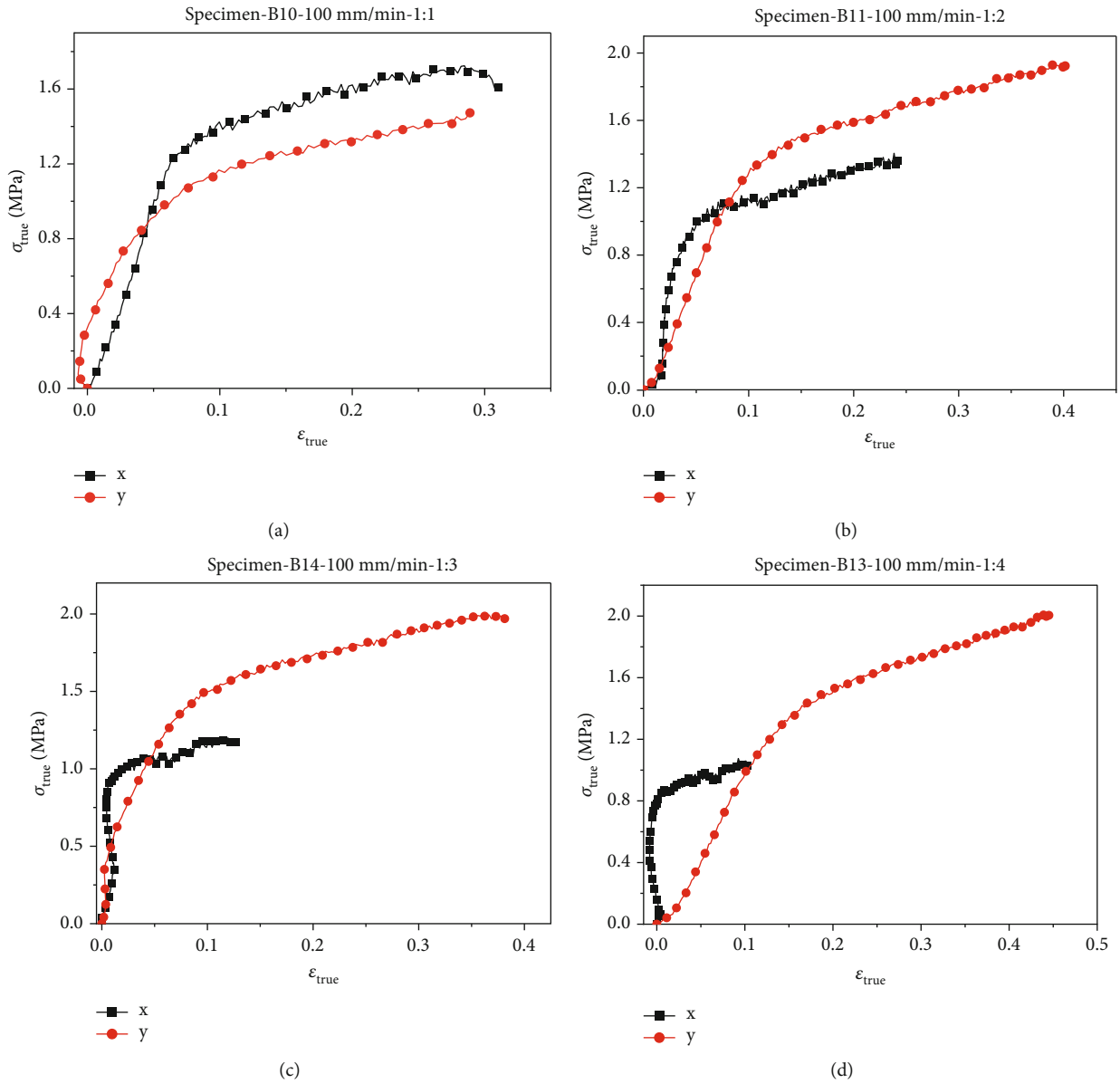

Figure 12: The true stress vs. strain curves of the biaxial tensile tests for HTPB propellant at 100 mm/min displacement loading speed: (a) the true stress vs. strain curve with loading rate ratio of 1 : 1, (b) the true stress vs. strain curve with loading rate ratio of 1 : 2, (c) the true stress vs. strain curve with loading rate ratio of 1 : 3, and (d) the true stress vs. strain curve with loading rate ratio of 1 : 4.

of the stress vs. time curves that correspond to the strain vs. time curves shown in Figure 8.

With true strain vs. time curves in Figure 8 and the true stress vs. time curves in Figure 11, the true stress vs. strain curves in X and Y direction, respectively, for all the specimens tested in the study could be obtained. Parts of the true stress vs. strain curves with four loading rate ratios for the specimens tested under the displacement loading speed of 100 mm/min are given in Figure 12.

3.4. The Equivalent Stress vs. Strain Curve. The uniaxial tensile stress and strain was obtained by uniaxial tensile test with test machine Zwick Z005. The true stress vs. true strain curves are shown in Figure 13.

The Mises equivalent stress vs. strain was used to analyze the tensile behavior of HTPB propellant. In this paper, the Mises stress refers neither to nominal nor true stress, but rather to an equivalent stress to the experimentally measured true stress. The Mises stress σ_e and strain ε_e formulas were given as

$$\sigma_e = \sqrt{\frac{1}{2}\left[(\sigma_1 - \sigma_2)^2 + (\sigma_1 - \sigma_3)^2 + (\sigma_2 - \sigma_3)^2\right]}. \quad (8)$$

The unit of stress σ_e is MPa.

$$\varepsilon_e = \sqrt{\frac{2}{9}\left[(\varepsilon_1 - \varepsilon_2)^2 + (\varepsilon_1 - \varepsilon_3)^2 + (\varepsilon_2 - \varepsilon_3)^2\right]}. \quad (9)$$

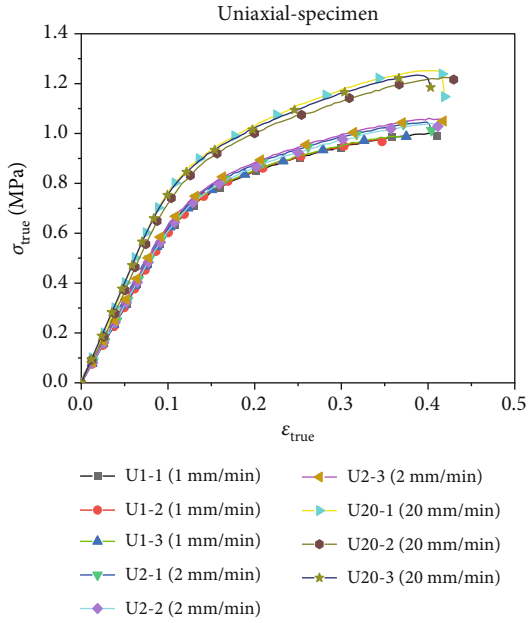

Figure 13: The uniaxial tensile stress vs. strain curve.

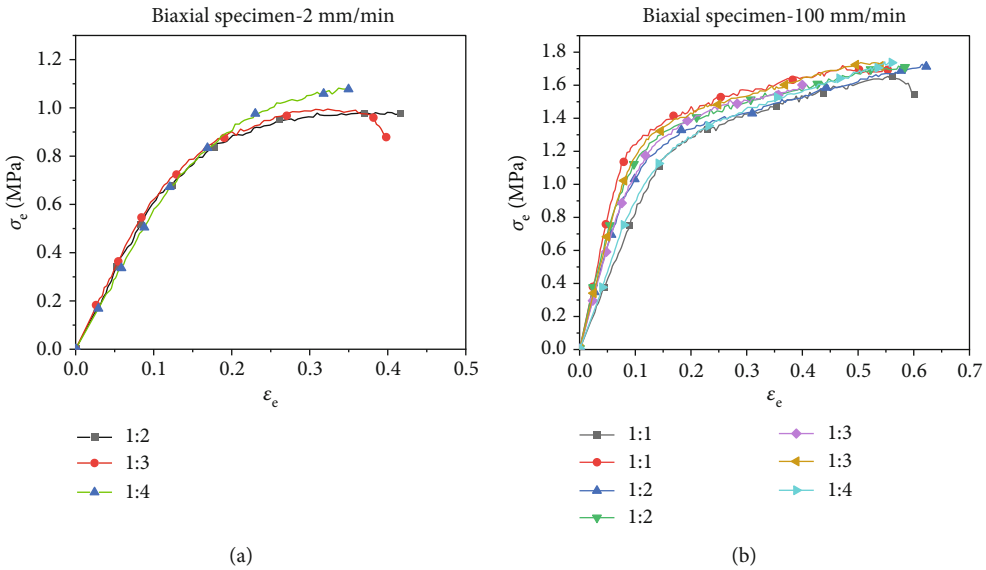

Figure 14: The biaxial tensile Mises equivalent stress vs. strain curves of HTPB propellant under the test conditions: (a) the Mises equivalent stress vs. strain curve at loading speed of 2 mm/min and (b) the Mises equivalent stress vs. strain curve at loading speed of 100 mm/min.

With the true stress vs. true strain curves in X and Y directions obtained for the specimens in the biaxial test as shown in Figure 12, the biaxial tensile Mises equivalent stress vs. strain curves of HTPB propellant under different test conditions could be obtained with Eqs. (8) and (9). The Mises equivalent stress vs. strain curves for specimens tested with two different loading speeds of 2 mm/min and 100 mm/min in the Y direction and different load ratios are shown in Figure 14. The biaxial equivalent stress vs. strain curves for various loading rate ratios exhibit a steady trend, as shown in Figure 14; however, the values vary slightly. The substance HTPB used in this study is a randomly filled composite that contains energy particles; therefore, there will obviously be some variability in the material itself. The mechanical behavior of the material will vary due to this inherent unpredictability, but this variability is acceptable for the purposes of this study.

With the test results shown in Figures 13 and 14, the following mechanical parameters were obtained according to the Chinese aerospace industry standard of P.R.C, GJB 770B-2005, and the American JANNAF standard. The uniaxial tensile elastic modulus $E(E_{bt})$ and biaxial equivalent modulus E_{bt} were defined in the conventional manner as the slope on the initial linear portion of the stress vs. strain curves in Figures 13 and 14. The maximum equivalent

Table 2: Mechanical parameters of uniaxial tensile test.

Experimental specimen and loading rate	Strain rate (s^{-1})	E_{bt} (MPa)	σ_{max} (MPa)	ε_{max}
U1-1 (1 mm/min)	2.3803E^{-4}	6.09424	1.00038	0.39985
U1-2 (1 mm/min)	2.3809E^{-4}	6.02940	0.97374	0.33743
U1-3 (1 mm/min)	2.3802E^{-4}	6.25598	0.98820	0.36212
U2-1 (2 mm/min)	4.7624E^{-4}	6.12434	1.04570	0.39847
U2-2 (2 mm/min)	4.7621E^{-4}	6.22063	1.04055	0.40425
U2-3 (2 mm/min)	4.7623E^{-4}	6.22066	1.06135	0.40061
U20-1 (20 mm/min)	4.7619E^{-3}	7.73921	1.25194	0.40832
U20-2 (20 mm/min)	4.7635E^{-3}	6.75688	1.22473	0.41672
U20-3 (20 mm/min)	4.7623E^{-3}	8.03057	1.23419	0.38733

Table 3: Mechanical parameters of biaxial tensile test under 2 mm/min displacement load.

Experimental specimen and loading rate ratio	Strain rate (s^{-1})	E_{bt} (MPa)	σ_{max} (MPa)	ε_{max}
B25 (1 : 2)	5.4395E^{-4}	6.27362	0.98351	0.36740
B24 (1 : 3)	5.3071E^{-4}	6.69363	0.99496	0.32305
B31 (1 : 4)	5.3036E^{-4}	5.78368	1.08179	0.33697

Table 4: Mechanical parameters of biaxial tensile test under 100 mm/min displacement load.

Experimental specimen and loading rate ratio	Strain rate (s^{-1})	E_{bt} (MPa)	σ_{max} (MPa)	ε_{max}
B10 (1 : 1)	0.05274	8.43696	1.65364	0.55391
B17 (1 : 1)	0.05120	15.73693	1.71876	0.47220
B11 (1 : 2)	0.04722	12.82369	1.72708	0.61596
B30 (1 : 2)	0.04500	15.32418	1.71602	0.57262
B9 (1 : 3)	0.03548	12.46207	1.60228	0.39973
B14 (1 : 3)	0.04039	13.60929	1.73712	0.50475
B13 (1 : 4)	0.03734	9.006280	1.74191	0.54794

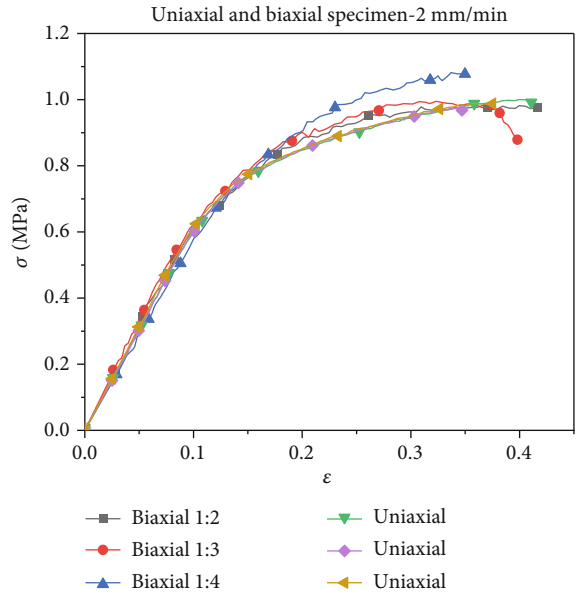

Figure 15: The biaxial Mises stress vs. strain curves and the uniaxial stress-strain curves.

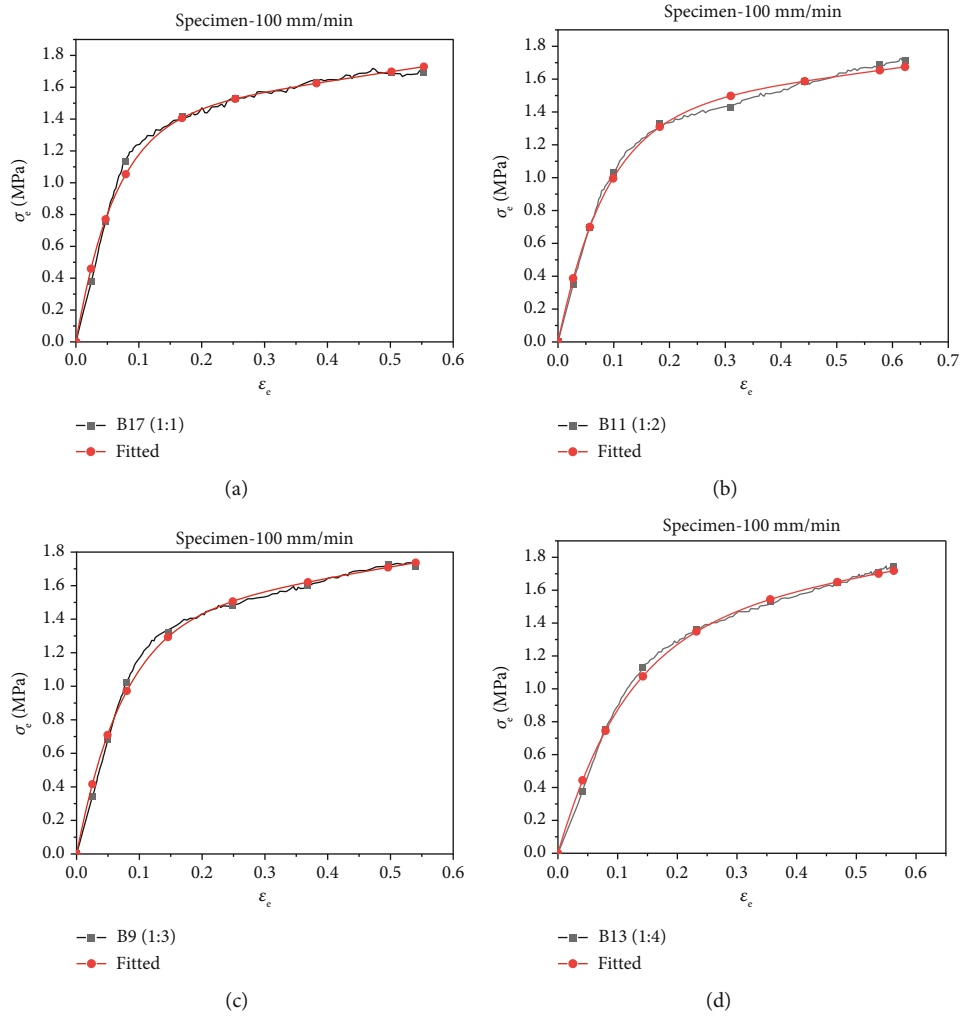

Figure 16: The biaxial tensile Mises stress vs. strain fitting curves of HTPB propellant: (a) curves at loading rate ratio of 1 : 1, (b) curves at loading rate ratio of 1 : 2, (c) curves at loading rate ratio of 1 : 3, and (d) curves at loading rate ratio of 1 : 4.

Table 5: Fitting parameters of HTPB propellant.

Experimental specimen	Strain rate (s^{-1})	A	B	C
U1-1	$2.3803E^{-4}$	0.8740	-1.4	-6.081
U1-2	$2.3809E^{-4}$	0.8653	-1.4	-6.095
U1-3	$2.3802E^{-4}$	0.8657	-1.4	-6.082
U2-1	$4.7624E^{-4}$	0.7839	-1.4	-6.201
U2-2	$4.7621E^{-4}$	0.7796	-1.4	-6.242
U2-3	$4.7623E^{-4}$	0.7848	-1.4	-6.221
B25	$5.4395E^{-4}$	0.7918	-1.4	-6.171
B24	$5.3071E^{-4}$	0.7941	-1.4	-6.195
B31	$5.3036E^{-4}$	0.7304	-1.4	-6.290
B10	0.05274	-0.4461	-1.4	-8.699
B17	0.05120	-0.5958	-1.4	-16.41
B11	0.04722	-0.4426	-1.4	-11.82
B30	0.04500	-0.5043	-1.4	-13.83
B9	0.03548	-0.5332	-1.4	-12.18
B14	0.04039	-0.6252	-1.4	-13.87
B13	0.03734	-0.5839	-1.4	-9.075

tensile stress σ_{max} and the corresponding equivalent strain ε_{max} were also obtained. Tables 2–4 list the mechanical parameters and the average equivalent strain rates under different loading condition, respectively.

It is shown from Figures 13 and 14 that the propellant displays nonlinear material behavior under all the test conditions. From Tables 2–4, it could be seen that the equivalent elastic modulus E_{bt}, the biaxial maximum tensile equivalent stress σ_{max}, and the corresponding equivalent strain ε_{max} increase with the increasing of the average strain rate. It could also be seen that under the same loading speed, the equivalent elastic modulus E_{bt}, the biaxial maximum tensile equivalent stress σ_{max}, and the corresponding equivalent strain ε_{max} did not relate with the loading rate ratios for biaxial tensile test results. It means that the biaxial tensile behaviors of HTPB propellant were remarkably influenced by loading rates but nearly not related with the loading rate ratios for biaxial tension experiment.

3.5. Discussion. The biaxial Mises equivalent stress vs. strain curves shown in Figure 14(a) and the uniaxial stress vs. strain curves tested under a loading speed of 2 mm/min are

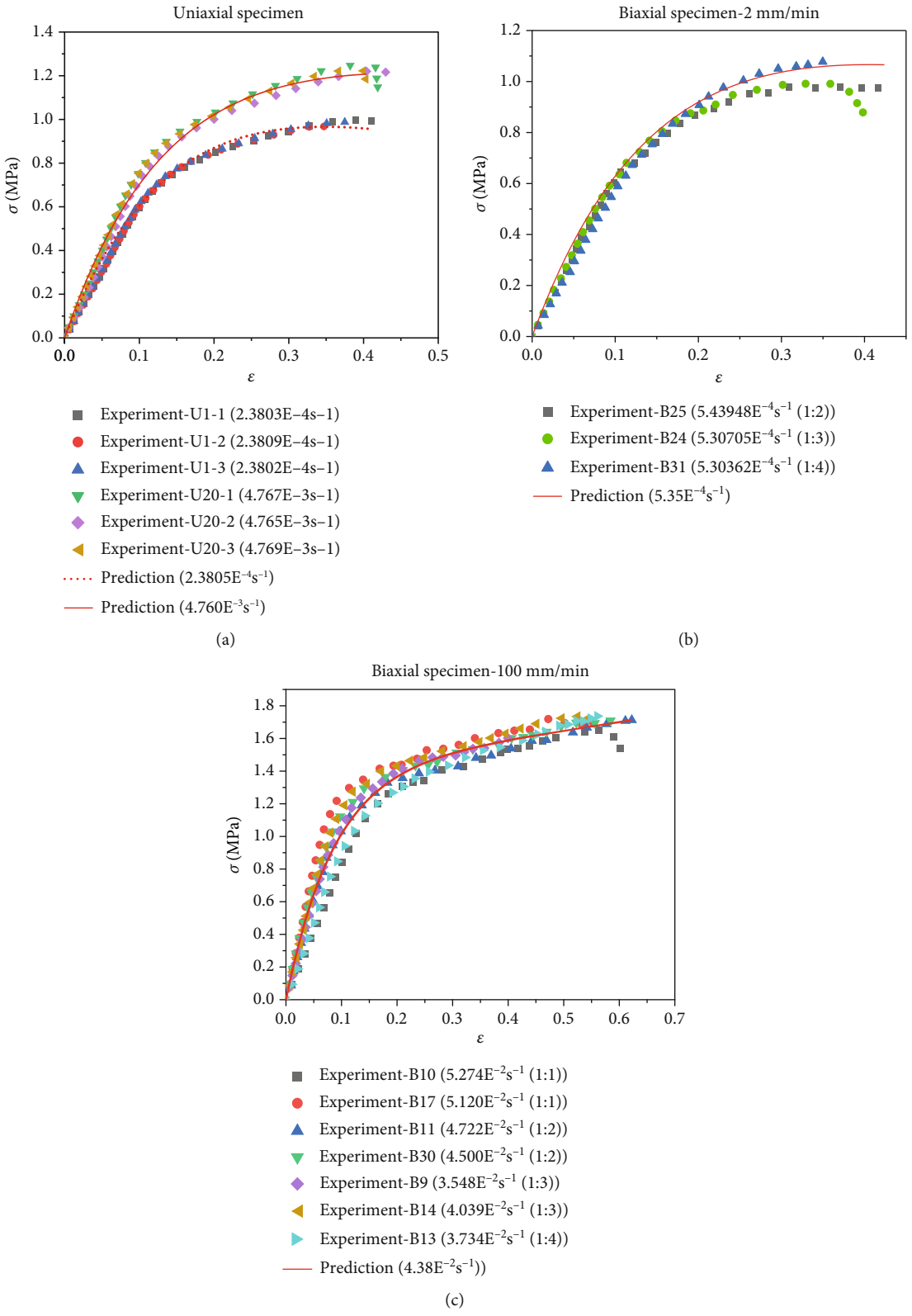

Figure 17: The comparison curve between calculated results and experimental results: (a) uniaxial tension of 20 mm/min, (b) biaxial tension of 2 mm/min, and (c) biaxial tension of 100 mm/min.

compared in Figure 15. It was shown that the uniaxial stress vs. strain curve and the Mises equivalent biaxial stress vs. strain curves could be approximately considered as the same. This meant that the Mises equivalent stress and strain could be approximately used to describe the biaxial tensile behaviors of the HTPB propellant material.

Eq. (8) shows an exponential function.

$$\sigma_e = (A\varepsilon_e + B)\left(e^{C\varepsilon_e} - 1\right), \quad (10)$$

where the A, B, and C were the corresponding fitting parameters.

All the stress vs. strain curves excluding the uniaxial tensile tests under loading speed of 20 mm/min would be fitted with Eq. (10). Figure 16 shows parts of the fitting curves, as follows.

It was found that the exponential function (Eq. (10)) could fit the stress vs. strain curve well in Figure 16. It was found that the fitting parameters value of B could be fixed as -1.4. The values of the fitting parameters are shown in Table 5.

It was found that the value of the fitting parameter A was linearly related to the strain rate $\dot{\varepsilon}$, and the value of the fitting parameter C was exponentially related to the strain rate $\dot{\varepsilon}$. Their fitting formulas were as follows:

$$A = -4.077\dot{\varepsilon}^{0.2278} + 1.493, \quad (11)$$

$$B = -1.400, \quad (12)$$

$$C = -136.3\dot{\varepsilon} - 6.174. \quad (13)$$

The unit of strain rate $\dot{\varepsilon}$ is s^{-1}.

Combined with the Eqs. (10), (11), (12), and (13), Eq. (14) could be obtained.

$$\sigma_e = \left(\left(1.493 - 4.077\dot{\varepsilon}^{0.2278}\right)\varepsilon_e - 1.4\right)\left(e^{-(136.3\dot{\varepsilon}+6.174)\varepsilon_e} - 1\right). \quad (14)$$

Figure 17(a) shows a comparison of the uniaxial stress vs. strain curve tested at a loading speed of 20 mm/min with the predict curve of Eq. (14). It was shown that although the Eq. (14) was obtained by the fitting results of all the stress vs. strain curves excluding the uniaxial tensile tests under loading speed of 20 mm/min, the predict curve with Eq. (14) fitted well with the experiment curves. The predict curves with Eq. (14) of other strain rates which correspond to the uniaxial tension of 1 mm/min, biaxial tension of 2 mm/min, and biaxial tension of 100 mm/min are also shown in Figures 17(a)–17(c), respectively.

It is shown from Figure 17 that the predict stress vs. strain curve obtained with Eq. (14) coincided well with the tested stress vs. strain curves of uniaxial tensile speed 1 mm/min and 20 mm/min, biaxial tension 2 mm/min, and biaxial tension 100 mm/min. It meant that Eq. (14) could be used to predict the stress vs. strain curve under different test conditions. It was also proved that Mises equivalent stress and strain could be used to describe the biaxial tension stress and strain state.

4. Conclusions

(a) The uniaxial tensile and biaxial tensile experiment for HTPB propellant was performed. It was shown that with the newly designed biaxial specimen, the stresses in the central part of the specimen were only related to the load acted on the arms of the specimen

(b) There were still some shortcomings in this article because the biaxial tensile stress values are obtained based on the linear constitutive model. Further calculations based on the constitutive model with damage were needed to more accurately reveal the changes in biaxial tensile mechanical behavior of solid propellants

(c) The elastic modulus E_{bt}, $\varepsilon_{\max}$, and $\sigma_{\max}$ increased with the increasing of the loading speed

(d) The Mises equivalent stress and strain could be used to describe the biaxial tension stress and strain state

(e) The constitutive model obtained in the study (Eq. (14)) could be used to predict the stress vs. strain curve under different test conditions

Data Availability

The data that support the findings of this study are available upon reasonable request from the authors.

Conflicts of Interest

The authors declare that they have no known competing financial interests or personal relationships that could have appeared to influence the work reported in this paper.

Authors' Contributions

Li Jin conceptualized the paper, conducted the methodology, wrote the original draft, and reviewed and edited the paper. Qin Zhi Fang wrote the original draft and reviewed and edited the paper. XingWei Yan conducted the investigation. Qin Wei Hu conducted the investigation.

Acknowledgments

This work is supported by the National Natural Science Foundation of China (11021202 and 11272244).

References

[1] R. Zalewski and T. Wolszakiewicz, "Analysis of uniaxial tensile tests for homogeneous solid propellants under various loading conditions," *Central European Journal of Energetic Materials*, vol. 8, no. 4, pp. 223–231, 2011.

[2] W. C. Jenkins, "Comparison of pressure and temperature stress-concentration factors for solid propellant grains," *Experimental Mechanics*, vol. 8, no. 2, pp. 94–96, 1968.

[3] H. C. Yildinm and S. Oezupek, "Structural assessment of a solid propellant rocket motor: effects of aging and damage," *Aerospace Science and Technology*, vol. 15, no. 8, pp. 635–641, 2011.

[4] Y. G. Xing, X. Y. Yang, K. H. Dong, and H. F. Liu, "Progress and prospect of the research on failure criterion for propellant

grains with defects in SRM," *Journal of Solid Rocket Technology*, vol. 27, no. 2, pp. 126–129, 2004.

[5] J. D. Burton, "Solid-propellant grain-to-case bond-stress measurement," *Experimental Mechanics*, vol. 10, no. 8, pp. 338–342, 1970.

[6] Y. Xing, Y. F. Li, K. H. Dong, and H. F. Liu, "Investigation for the critical size of debond in a solid rocket motor of end burning," *Journal of Solid Rocket Technology*, vol. 26, no. 4, pp. 48–51, 2003.

[7] S. J. Bennett and G. P. Anderson, "Failure properties of a PBAN propellant in multiaxial stress fields," *Experimental Mechanics*, vol. 8, no. 9, pp. 411–417, 1968.

[8] R. S. Xing, L. Wang, F. T. Zhang, and C. T. Hou, "Mechanical behavior and constitutive model of NEPE solid propellant in finite deformation," *Mechanics of Materials*, vol. 172, article 104383, 2022.

[9] P. A. Kakavas-Papaniaros, "On the distribution of particles in propellant solids," *Acta Mechanica*, vol. 231, no. 3, pp. 863–875, 2020.

[10] W. Zhao, K. Han, W. Xu, and C. Liu, "Uniaxial and quasi-biaxial tensile mechanical properties of aged HTPB propellant at low temperatures under dynamic loading," *Journal of Solid Rocket Technology*, vol. 41, no. 5, pp. 593–596, 2018.

[11] R. Zalewski, T. Wolszakiewicz, and J. Bajkowski, "Effect of temperature on fundamental mechanical properties of homogeneous solid propellants," *Przemysl Chemiczny*, vol. 91, no. 9, pp. 1830–1833, 2012.

[12] L. Gong, Y. H. Li, Y. P. Guo, J. M. Li, and R. J. Yang, "Effect of morphology for ammonium dinitramide on the mechanical and combustion properties of composite propargyl-terminated copolyether propellant," *Propellants Explosives Pyrotechnics*, vol. 45, no. 6, pp. 864–870, 2020.

[13] Z. Wang, H. F. Qiang, G. Wang, and X. L. Chang, "Review on the mechanical properties and constitutive models of solid propellants," *Chinese Jouranal of Energetic Materials*, vol. 24, no. 4, pp. 403–416, 2016.

[14] H. Li, J. S. Xu, H. L. Wang, and C. S. Zhou, "Research on the safety mechanical properties of beehive propellant grain in SRM," *Computer Simulation*, vol. 34, no. 4, pp. 100–104, 2017.

[15] J. M. Nelson and W. Stibor, "Three-dimensional photoelastic and finite-element analysis of a propellant grain," *Experimental Mechanics*, vol. 12, no. 9, pp. 436–440, 1972.

[16] P. Ren, X. Hou, and G. R. He, "Comparative research of tensile and compressive modulus of composite solid propellant for solid rocket motor," *Journal of Astronautics*, vol. 31, no. 10, pp. 2354–2359, 2010.

[17] Y. Traissac, J. Ninous, R. Neviere, and J. Pouyet, "Mechanical behavior of a solid composite propellant during motor ignition," in *Toughened Plastics II: Novel Approaches in Science and Engineering*, C. K. Riew and A. J. Kinloch, Eds., pp. 195–210, ACS Publications, 1996.

[18] A. San Miguel and E. N. Duran, "On the measurement of stress in solid propellant," *Experimental Mechanics*, vol. 10, no. 12, pp. 514–520, 1970.

[19] G. A. Gazonas and J. C. Ford, "Unixial compression testing of M30 and JA2 gun propellants using a statistical design strategy," *Experimental Mechanics*, vol. 32, no. 2, pp. 154–162, 1992.

[20] L. G. Duan, G. Wang, G. X. Zhang, X. Y. Sun, and H. H. Shang, "A investigation on unixial and quasi-biaxial tensile mechanical properties of aging HTPB propellant under dynamic loading at low temperature," *AIP Conference Proceedings*, vol. 1971, article 050007, 2018.

[21] C. Liu, Z. J. Wang, H. F. Qiang, and W. C. Xu, "Thermal aged properties of HTPB propellant at low temperature under dynamic quasi-biaxial tensile loading," *Journal of Astronautics*, vol. 41, no. 3, pp. 353–361, 2020.

[22] O. K. Garishin and V. V. Shadrin, "Testing mechanical features of rubber composites under biaxial loading," *IOP Conference Series: Materials Science and Engineering*, vol. 581, no. 1, article 012025, 2019.

[23] F. F. Zhang, Z. M. Wan, and X. W. Du, "Mechanical properties of Nylon6 cord-rubber composite subjected to biaxial tensile loads," *Journal of Elastomers and Plastics*, vol. 34, no. 3, pp. 265–278, 2002.

[24] A. Kossa, "A new biaxial compression fixture for polymeric foams," *Polymer Testing*, vol. 45, pp. 47–51, 2015.

[25] D. J. Zhu, B. Mobasher, A. Vaidya, and S. D. Rajan, "Mechanical behaviors of Kevlar 49 fabric subjected to uniaxial, biaxial tension and in-plane large shear deformation," *Composites Science and Technology*, vol. 74, pp. 121–130, 2013.

[26] Z. Wang, H. F. Qiang, G. Wang, and T. J. Wang, "A new test method to obtain biaxial tensile behaviors of solid propellant at high strain rates," *Iranian Polymer Journal*, vol. 25, no. 6, pp. 515–524, 2016.

[27] S. Bruschi, T. Altan, D. Banabic et al., "Testing and modelling of material behaviour and formability in sheet metal forming," *Cirp Annals Manufacturing Technology*, vol. 63, no. 2, pp. 727–749, 2014.

[28] T. Kuwabar, "Advances in experiments on metal sheets and tubes in support of constitutive modeling and forming simulations," *International Journal of Plasticity*, vol. 23, no. 3, pp. 385–419, 2007.

[29] W. Liu, D. Guines, L. Leotoing, and E. Ragneau, "Identification of sheet metal hardening for large strains with an in-plane biaxial tensile test and a dedicated cross specimen," *International Journal of Mechanical Sciences*, vol. 101-102, pp. 387–398, 2015.

[30] N. Srinicasan, R. Velmurugan, and R. Kumar, "Deformation behavior of commercially pure (CP) titanium under equi-biaxial tension," *Materials Science and Engineering A*, vol. 674, pp. 540–551, 2016.

[31] Y. Jia and W. Zhang, "Optimal design and examination study of biaxial tensile specimens for solid propellant," *Journal of Propulsion Technology*, vol. 32, no. 5, pp. 737–740, 2011.

[32] A. Barroso, E. Correa, J. Freire, and F. París, "A device for biaxial testing in uniaxial machines. Design, manufacturing and experimental results using cruciform specimens of composite materials," *Experimental Mechanics*, vol. 58, no. 1, pp. 49–53, 2018.

[33] K. Renganathan, B. S. V. Rama Sarma, B. Nageswara Rao, M. K. Jana, and K. Renganathan, "Tensile fracture of HTPB based propellant specimens," *Materials Science and Technology*, vol. 18, no. 11, pp. 1408–1412, 2002.

[34] G. M. Hommer, J. S. Park, P. C. Collins, A. L. Pilchak, and A. P. Stebner, "A new in situ planar biaxial far-field high energy diffraction microscopy experiment," *Advancement of Optical Methods in Experimental Mechanics*, vol. 3, pp. 61–70, 2017.

[35] T. J. Geng, H. F. Qiang, Z. J. Wang, X. R. Wang, Z. J. Zhu, and D. Qiao, "Macroscopic and mesoscopic properties of HTPB

propellant under low temperature dynamic biaxial compression loading," *Polymer Testing*, vol. 119, article 107922, 2023.

[36] H. Hamori, H. Kumazawa, R. Higuchi, and T. Yokozeki, "Gas permeability of CFRP cross-ply laminates with thin-ply barrier layers under cryogenic and biaxial loading conditions," *Composite Structures*, vol. 245, article 112326, 2020.

[37] D. Jalocha, A. Constantinescu, and R. Neviere, "Prestrained biaxial DMA investigation of viscoelastic nonlinearities in highly filled elastomers," *Polymer Testing*, vol. 42, pp. 37–44, 2015.

[38] A. Makinde, L. Thibodeau, and K. W. Neale, "Development of an apparatus for biaxial testing using cruciform specimens," *Experimental Mechanics*, vol. 32, no. 2, pp. 138–144, 1992.

[39] A. F. Liu, J. E. Allison, D. F. Dittmer, and J. R. Yamane, "Effect of biaxial stresses on crack growth," in *Fracture Mechanics*, pp. 5–22, ASTM Special Technical Publication, 1979.

[40] Q. Z. Fang, T. J. Wang, and H. M. Li, "Large tensile deformation behavior of PC/ABS alloy," *Polymer*, vol. 47, no. 14, pp. 5174–5181, 2006.

[41] Q. Xu, Q. Z. Fang, B. L. Sha, and Q. W. Hu, "Study on a damage model of NEPE solid propellant based on a Weibull distribution," *Mechanics of Time-Dependent Materials*, vol. 27, no. 1, pp. 19–34, 2023.